A Compact Sideband Separating Downconverter With Excellent Return Loss and Good Conversion Gain for the W Band

David Monasterio, Claudio Jarufe, Diego Gallardo, Nicolas Reyes, Fausto Patricio Mena, and Leonardo Bronfman

***Abstract*—We have developed a sideband separating receiver module for the *W* band (75–110 GHz) that has been designed with a scalable and compact architecture allowing easy integration into larger systems, like focal plane arrays. The receiver includes a high-frequency amplification stage giving it a good conversion gain and, most importantly, due to its original architecture, excellent return losses. The latter permits, if needed, efficient incorporation of further amplification prior to mixing. The module is based on a 90° hybrid followed by an amplification stage and broadband mixers. As amplification stage, we rely on commercial low-noise amplifier chips that use the 70-nm metamorphic-high-electron-mobility process from OMMIC. The downconverter is a subharmonic mixer designed as a monolithic microwave integrated circuit and fabricated using the standard gallium-arsenide Schottky diode process from United Monolithic Semiconductor. The size of the module is 50 mm × 25 mm × 20 mm and shows good performance with an input return loss above 12 dB in the entire band, an average conversion gain of 5 dB, and sideband rejection ratio above 10 dB in the majority of the band. The primary motivation of this article has been radio astronomy, but other areas like imaging, telecommunications, or remote sensing can benefit from such compactness and integrability into multibeam systems.**

***Index Terms*—Focal plane arrays (FPAs), frequency conversion, low-noise amplifiers, microwave integrated circuits, microwave mixers, multibeam systems, multichip modules.**

Manuscript received June 14, 2019; revised August 13, 2019; accepted August 14, 2019. Date of publication August 27, 2019; date of current version November 4, 2019. This work was supported in part by the Chinese Academy of Sciences, South American Center for Astronomy and in part by the CONICYT project Basal AFB-170002. The work of D. Monasterio was supported in part by CONICYT-PFCHA/Doctorado Nacional/2019-21190632. *(Corresponding author: David Monasterio.)*

D. Monasterio, D. Gallardo, and F. P. Mena are with the Department of Electrical Engineering, Universidad de Chile, Santiago 8370451, Chile (e-mail: david.monasterio@raig.uchile.cl; diego.gallardovives@gmail.com; fpmena@uchile.cl).

C. Jarufe was with the Department of Electrical Engineering, Universidad de Chile, Santiago 8370451, Chile. He is now with the School of Electrical and Electronic Engineering, University of Manchester, Manchester M13 9PL, U.K. (e-mail: claudio.jarufe@raig.uchile.cl).

N. Reyes is with the Department of Electrical Engineering, Universidad de Chile, Santiago 8370451, Chile, and also with the Max Planck Institute fur Radioastronomie, Bonn 53121, Germany (e-mail: nireyes@uchile.cl).

L. Bronfman is with the Department of Astronomy, Universidad de Chile, Santiago 8370451, Chile (e-mail: leo@das.uchile.cl).

Color versions of one or more of the figures in this article are available online at http://ieeexplore.ieee.org.

Digital Object Identifier 10.1109/TTHZ.2019.2937955

I. Introduction

INTEREST in constructing focal plane arrays (FPAs) has been growing over the last few years. The potential of simultaneous detection using a large number of receiver elements make them very interesting for applications such as radio astronomy, millimeter wave imaging systems, satellite communications, and earth remote sensing [1]–[4]. To achieve high-density multibeam systems, receivers need to be compact. In fact, their construction has been changing from using discrete components to more modular designs with higher level of integration [5]. As part of this effort, several compact modules that incorporate one or more low noise amplifiers (LNAs) in front of a down-converting stage have been developed. In [6], a *W* band low noise receiver that could be used as 2SB receiver is presented, although no measurements of image rejection are provided. The module is intended for cryogenic operation. When cooled down, the noise is 33 K in average and its gain is above 15 dB. A double sideband receiver module from 140 to 180 GHz is presented in [7]. In cryogenic operation, measured noise temperature and gain are above 50 K and 10 dB, respectively. In both devices, it is not possible to separate the high-frequency amplification from the down-converting stages. This characteristic can become a drawback for some applications. For example, radio astronomical applications require the LNA to operate at low temperatures. Therefore, in FPAs with a high number of pixels, due to cooling restrictions and to provide easier replacement of components, it would be more advantageous to have the down-converting stage separated from the LNA while maintaining a compact design. A 2SB Schottky receiver is presented in [4] that works from 320 to 370 GHz integrating two subharmonic mixers followed by low frequency LNAs. It shows an image rejection better than 15 dB at 340 GHz and a noise figure above 10 dB. The main limitations of this receiver are that the loads for the isolated ports are not included in the block and its reduced fractional bandwidth. Furthermore, no measurement of the input return loss for the RF path is presented.

In this article, we present the design and construction of a low-noise downconverter module with good gain and excellent input return loss. Although it has been designed for use with a spectrometer that implements the IF hybrid digitally, it can work in a 2SB configuration by adding an external low-frequency hybrid. The module was designed with a scalable and compact

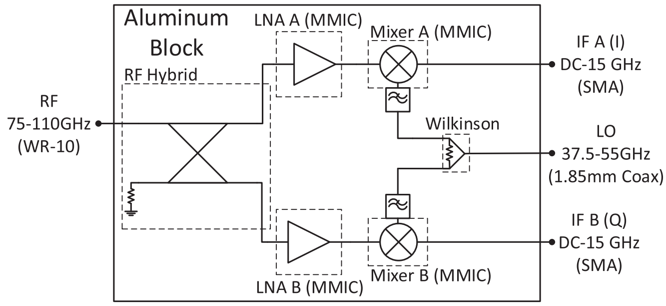

Fig. 1. Architecture of the broadband downconverter. The input quadrature coupler allows the module to be used as sideband separation mixer. The first amplification stage is a 20-dB MMIC from OMMIC. The second stage is the downconverter itself, which is implemented as a subharmonic mixer. The LO is distributed using a Wilkinson coupler followed by an LO filter.

architecture that allows easy integration into larger systems. This article is focused in the band from 75 to 110 GHz motivated by several astronomical projects, including the Atacama Large Millimeter Array, and the possible upgrade of the TianMa Shanghai Radiotelescope to the *W* band using FPAs. However, multiple areas outside astronomy can benefit from such compactness and feasibility of integration. The module presents noise below 10 dB, input return loss above 12 dB, and gain above 5 dB over most of the design bandwidth. When a low-frequency hybrid is added, a sideband separation ratio above 7 dB can be obtained, although it could be improved up to 40 dB by using a digital IF hybrid [8].

II. Module Design and Construction

The module is based on an RF hybrid followed by a high-frequency amplification stage and broadband mixers. Fig. 1 presents a schematic of the downconverter. The input stage is a quadrature hybrid implemented in WR10 waveguide with the isolated port terminated in an integrated waveguide load. Each signal is amplified by a commercial LNA and then down converted using subharmonic mixers. The latter were designed in-house and built in monolithic microwave integrated circuit (MMIC) commercial technology using gallium-arsenide (GaAs) Schottky diodes [10]. The *I* (in-phase) and *Q* (quadrature) output IF signals have a broadband range from 0.1 to 12 GHz. The local oscillator (LO) signal required by the mixer is delivered by a Wilkinson divider followed by a low-pass filter that acts as a controlled termination for RF signals leaking into the LO path. As demonstrated in the following, this architecture allows obtaining better input return losses compared to the reflections of LNAs, as long as they are not too different.

To simplify the analysis, and referring to Fig. 2(a), it is assumed that the hybrid has no reflections, and that the backward transmissions of the LNAs are low enough so that they become the main source of reflections. Under these assumptions, the amplitude of the reflected wave at the RF port can be written as

$$\left|V_{\mathrm{RF}}^{\mathrm{Reff}}\right|^2 = A^2 + B^2 - 2AB\cos\left(\Delta_A - \Delta_B\right) \quad (1)$$

where $A = \gamma_A V_0 \rho_A^2$, $B = \gamma_B V_0 \rho_B^2$, $\Delta_A = 2\varphi_A + \theta_A$, and $\Delta_B = 2\varphi_B + \theta_B$. $\gamma_{A,B}$ and $\theta_{A,B}$ are the magnitude and phase of the reflection coefficients of LNAs *A* or *B*, $\rho_{A,B}$ and $\varphi_{A,B}$ are

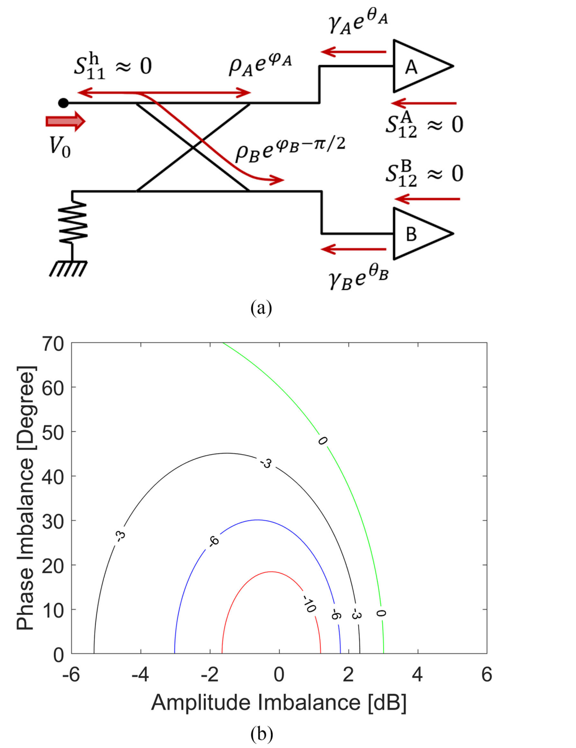

Fig. 2. (a) Flow graph for the return loss of the module. Reflections of the hybrid, R_{11}^h, and backward transmissions of the amplifiers, $S_{12}^{A,B}$, are neglected. Because of the latter, reflections from the rest of the system are of no importance. (b) Improvement, in dB, of the reflected wave $|A|^2$ when adding the 90° RF hybrid at the input for unbalanced systems. From the center, the curves are at -10, -6, -3, and 0 dB.

the magnitude and phase (relative to an ideal hybrid) of the transmission coefficients of the RF hybrid to LNAs *A* or *B*, and V_0 is the amplitude of the input RF signal. Note that quantities A and B represent the amplitudes of the reflected waves from LNAs *A* and *B*, considering only the transmission of the hybrid.

In a perfectly balanced configuration both LNAs would be identical, implying $A = B$ and $\Delta_A = \Delta_B$, and, therefore, $|V_{\mathrm{RF}}^{\mathrm{Reff}}|^2 = 0$. In other words, no power is reflected to the input port. The situation when there is no perfect balance is shown in Fig. 2(b). This figure presents the ratio (in dB) of the reflected wave $|V_{\mathrm{RF}}^{\mathrm{Reff}}|^2$ to $|A|^2$ in terms of amplitude and phase imbalances. Thus, the plot represents the improvement of S_{11} of the entire system with respect to the reflection caused by taking into account only the amplifier *A*. The graph is mirrored about the *Y*-axis when plotting the improvement with respect to amplifier *B*. Therefore, for small imbalances, improved S_{11} will be obtained in comparison to both amplifiers, *A* and *B*. However, with higher levels of imbalances, S_{11} will improve only compared to one of the amplifiers, either *A* or *B*.

The module does not include an IF hybrid as it was designed for use with modern digital spectrometers that implement it digitally [8]. However, an external low frequency hybrid can be added to separate the upper and lower sidebands. The usual mathematical analysis, e.g., see [9], does not include the effect of the LNAs, but their effect can be easily taken into account by adding their gain and phase imbalances. They will add up to the imbalances of the other components of the system. However,

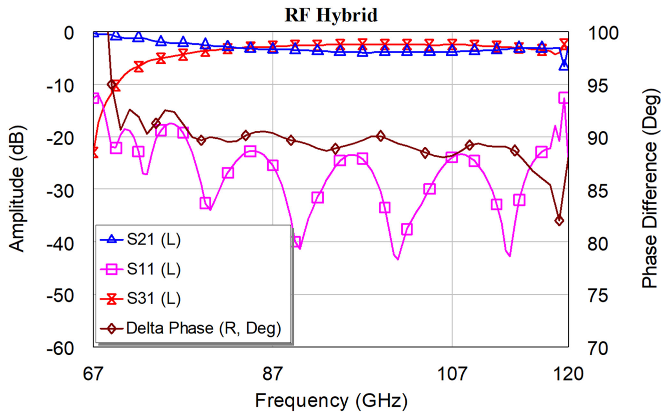

Fig. 3. Scattering parameters of the multibranch waveguide 90° hybrid simulated in HFSS.

since the gain of the amplifiers can be tuned by changing the bias of the LNAs, so can the sideband separation.

A. Waveguide Coupler and Load

The multibranch waveguide 90° hybrid was designed in ANSYS HFSS with the goal of achieving minimum amplitude and phase imbalance performance over all the extended *W* band (67–115 GHz). However, restrictions on the minimum width of the branches were imposed in order to match our current capabilities of fabrication. The simulation results are presented in Fig. 3. They indicate that the bandwidth performance is limited by the restrictions imposed on the design. Therefore, the upper side of the band was preferred because of its scientific importance in radio astronomy. The load necessary to terminate the hybrid was integrated to the design and implemented using MF-124 from ECCOSORB.

B. LNAs

The commercial LNA CGY2190 from OMMIC [11] was used to improve the sensitivity of the module. This MMIC is a four-stage amplifier based on a 70-nm metamorphic-high-electron-mobility-transistor. The conduction channel has a high percentage of indium content, achieving a low noise operation and high cutoff frequencies. The power consumption of the chip is about 30 mW, which is not a problem for room temperature operation.

The MMIC was packaged in a test block to measure noise and gain at room temperature. A picture of the mounted MMIC on the test block is presented in Fig. 4(a). Measurements presented in Fig. 4(b), show an average gain and noise of 18.5 dB and 626 K, respectively, on the *W* band. The amplifier covers the band of interest with a roll off at the band edges. The measurement shows higher noise and lower gain than the values provided by the manufacturer [11] but this is expected because of the effects of the packaging.

C. Mixers

The central element in a heterodyne receiver is the mixer. Considering the number of mixers needed in an FPA it is very important that the mixers require low LO power. To simplify LO routing and reduce the number of bias lines we decided to use unbiased subharmonic mixers. The mixer chips were designed using the GaAs process from United Monolithic Semiconductors (BES) [9] which has shown a good performance in the *W* band [12].

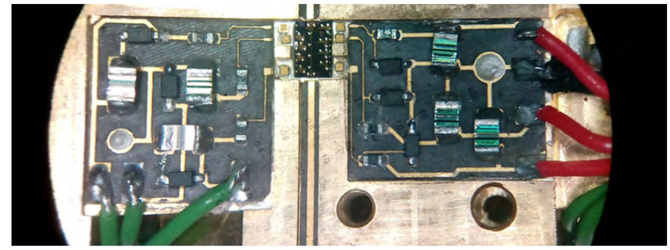

(a)

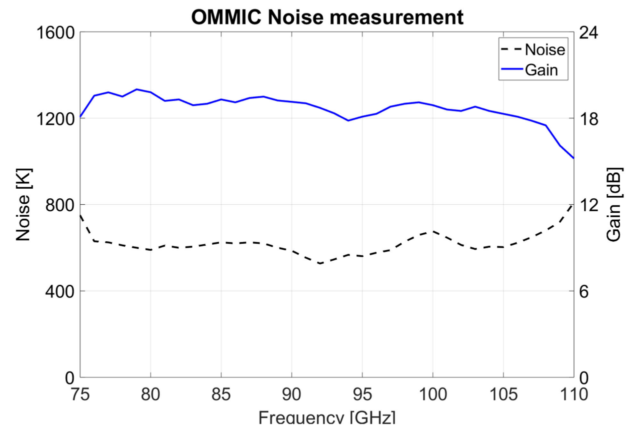

(b)

Fig. 4. LNA CGY2190 from OMMIC. (a) Picture of the amplifier packaged with a microstrip line as input and output in a test block. (b) Measured gain (solid blue) and noise (dashed black) at room temperature.

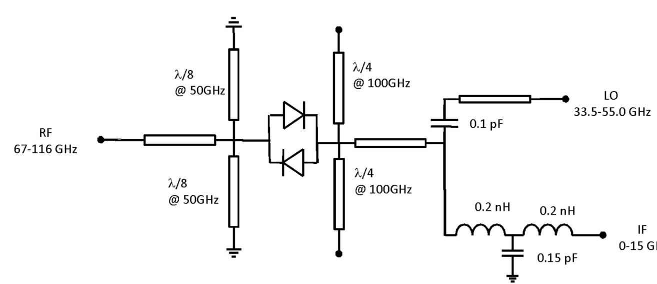

Fig. 5. Schematic of the subharmonic mixer.

An antiparallel diode configuration connected in series between the RF port and the LO and IF ports [13] was used in the design. Because they use only odd intermodulation products, the LO frequency is half of that of the RF signal. The mixer was designed in AWR Microwave Office [14] to have an ultra-wide band RF frequency between 67 and 116 GHz, an LO frequency between 33.5 and 55 GHz, and an IF frequency between dc and 15 GHz. Fig. 5 presents a schematic diagram of the mixer implementation. A $\lambda_{\mathrm{RF}}/4$ dual open stub is used to terminate the RF input in a virtual short, but allowing the LO and IF signals to propagate. On the RF side, the IF and LO signals

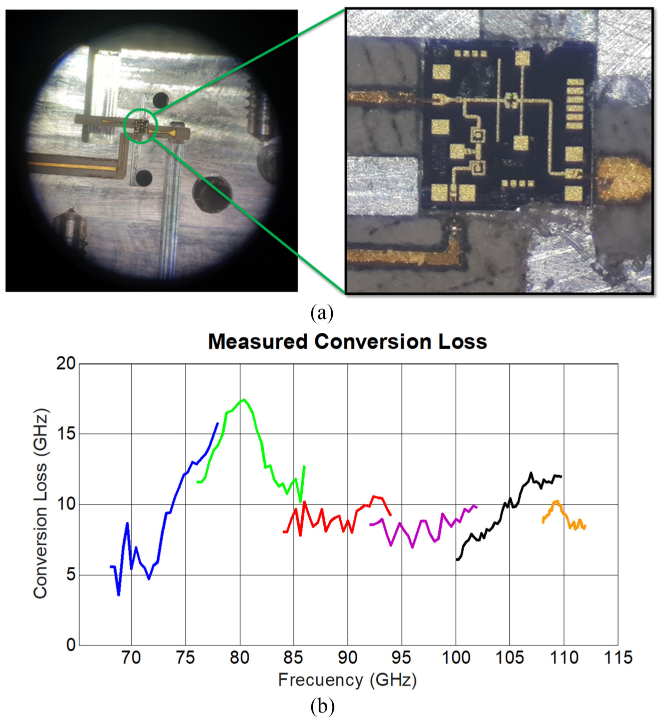

Fig. 6. MMIC mixer. (a) Photograph of the MMIC packaged in a test block. (b) Measured conversion losses for a LO frequency of 34, 38, 42, 46, 50, and 54 GHz with an average power of 5 dBm.

are terminated in a $\lambda_{LO}/8$ short stub. This configuration allows the RF frequency to propagate into the diodes, but not the LO and IF frequencies into the RF port. Ideally the LO termination should be a $\lambda_{LO}/4$ open stub, but to reduce the size of the chip we decided to use a $\lambda_{LO}/8$ short stub, that acts as a high-pass filter at the RF frequency. The LO and RF terminations were placed as close to the diodes as possible. In order to achieve a good isolation between the IF and LO ports, a high-pass filter (series capacitor) was used in the LO input and a low-pass filter (L-C-L in tee configuration) was used in the IF output.

The mixer was fabricated at united monolithic semiconductors (UMS) and assembled in a test fixture as seen in Fig. 6(a). Measurements presented in Fig. 6(b), show conversion losses between 10 and 18 dB when operated with an LO power between 4 and 6 dBm. An increase of the conversion loss at 80 GHz that did not appear in the original design was identified. Using simulation tools, we identified this effect as caused by RF power that is not properly terminated at the RF termination. This problem is originated by the RF termination being tuned at 100 GHz and being not optimal at the lower end of the band. The performance of the mixer can be improved by using a different implementation of the RF short in the MMIC. The bandwidth can increase using a double radial stub instead of double linear one [15].

D. Wilkinson Power Divider and LO Filter

A microwave power divider was implemented to split the LO signal to the two mixers. The power divider selected to accomplish this task was a microstrip Wilkinson power divider.

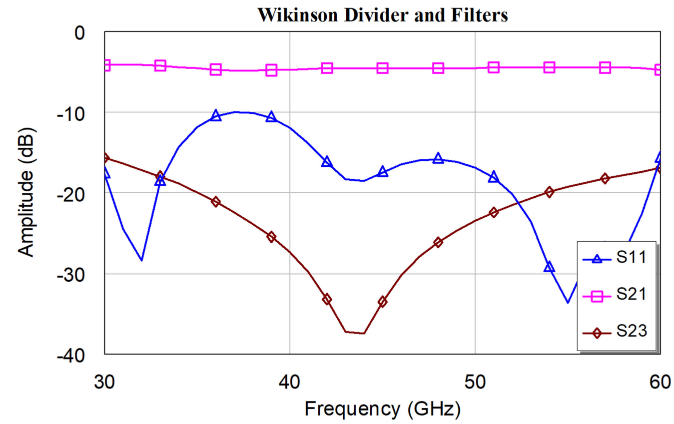

Fig. 7. Scattering parameters of the Wilkinson divider and filters simulated in HFSS.

This type of divider has good isolation between its output ports, a necessary feature to avoid standing waves between the two mixers caused by the high reflections of the LO port.

The Wilkinson divider was implemented in Rogers Duroid 6202, with a thickness of 127 μm. A 50-GHz 100-Ω resistor from Vishay Intertechnology in a 0201-package format CH02016 was used to implement the necessary resistor. The input and output ports are matched to 50 Ω. At the output port, low-pass radial stub filters were placed in order to control reflections from the leaked RF power to the LO port.

The complete Wilkinson divider, including the filters, was simulated using HFSS. Simulation results presented in Fig. 7, show an isolation of 15 dB and an input return loss better than 10 dB in the complete band. However, the selected resistor decreases its $|Z|/R$ ratio above 50 GHz [17] which, in turn, could cause problems above this frequency. They could manifest in low isolation and matching of the two output ports of the Wilkinson. Since it is known that the LO port of the mixer has a high reflection coefficient, a standing wave can be generated with either the divider (due to the poor match) or the other mixer (due to poor isolation). This standing wave will generate regions in the bandwidth where the LO power needed to drive the mixers is increased.

E. Simulations of the Entire Downconverter Module

The complete module was simulated using the nonlinear harmonic-balance legacy simulator of AWR Microwave Office. The simulated scattering parameters of several components (particularly the RF hybrid and Wilkinson divider) were imported from HFSS. The amplifier was simulated using the scattering parameters provided by the manufacturer. Since the module requires an external IF coupler to work as a sideband separating mixer, for simulation purposes, an ideal IF hybrid was added to the model. Fig. 8 shows the simulated conversion gain of the module in a sideband-separating configuration in both the upper sideband (USB) and lower sideband (LSB). Additionally, Fig. 9 shows the return loss for the entire bandwidth and Fig. 10 the sideband rejection ratio (SRR).

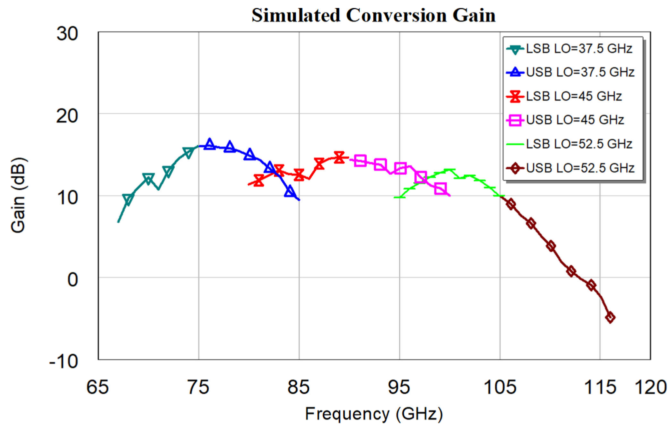

Fig. 8. Simulated conversion gain of the entire module in AWR with an average LO power of 9 dBm.

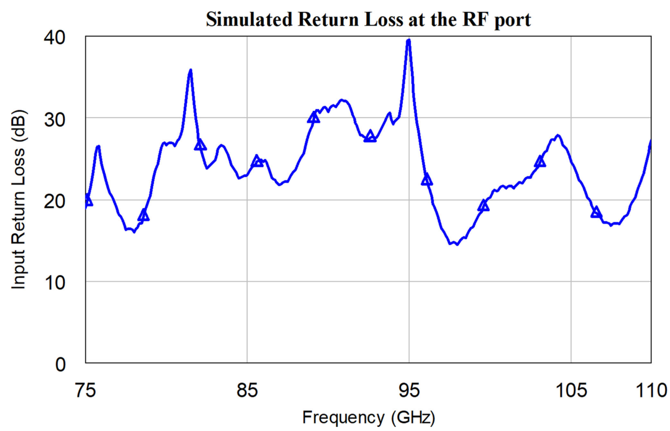

Fig. 9. Simulated return loss of the module in AWR.

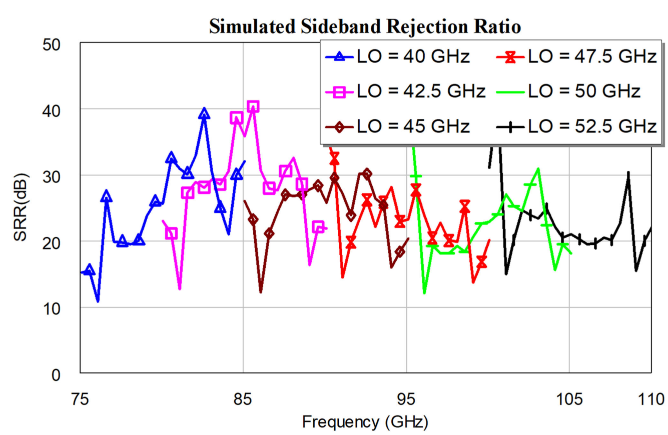

Fig. 10. Simulated sideband rejection ratio in AWR.

The simulations show very good performance over the entire frequency range, with a decrease in conversion gain at the end of the band. This phenomenon is due to the reduced gain of the LNA at the high end of the band and to the existence of a long-period standing wave between the amplifier and the mixer. The return loss is above 15 dB in the entire band and it is not significantly affected by the LO signal injected into the mixer.

TABLE I
ESTIMATED AVERAGE NOISE AND GAIN OF THE MODULE

COMPONENT	GAIN [dB]	NOISE FIGURE [dB]	ACCUMULATED NOISE [dB]
RF HYBRID	–3	1.81	1.81
LNA	18.5	4.87	7.5
MIXER	–10	10	7.7
MODULE	5.5	7.7	-

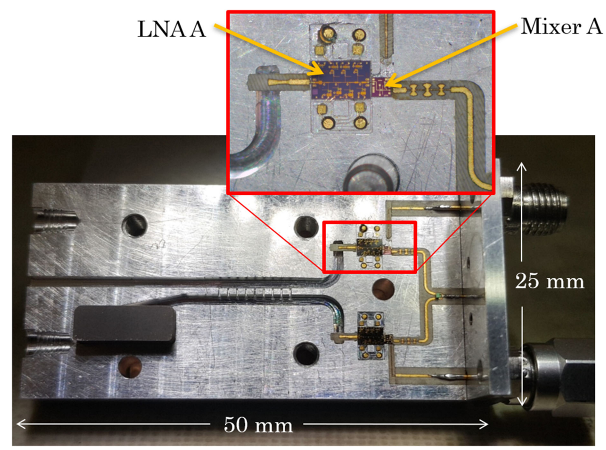

Fig. 11. Picture of the interior of the assembled module. The inset shows details of the MMICs containing the LNA and mixer, respectively.

Table I summarizes an estimated average value, for the *W* band, of the noise figure for the different stages of the module. The last row of the table shows an estimated value for the noise of the entire module for the I/Q branches. This estimation was made using the Friis formula for noise [16]. This value will decrease significantly if a cryogenic amplifier of high gain is placed before module.

F. Construction and Assembly of the Module

The housing, which includes all waveguide structures, was fabricated on Aluminum 6061 using a high-precision CNC milling machine. The tool available for the construction of the slots of the hybrid, which is the most sensitive part of the structure, has a diameter of 0.2 mm and a height of 1.3 mm. The height-to-diameter ratio is extremely high, thus giving an important constraint in the design of the hybrid and its bandwidth.

The size of the final block is 50 mm × 25 mm × 20 mm. Its height is set by the input RF connector, a rectangular waveguide (WR10). The LO is fed using a 1.85-mm connector and the IF signals are transmitted using SMA connectors. For biasing the amplifier, the module uses a 15-pin connector. In the backside of the block, a bias circuit provides overvoltage protection using Zener diodes. This circuit is connected to the interior of the block with dc feedthroughs from Emerson Thunderline Z.

Fig. 11 shows a photograph of the constructed module. As it can be seen in the picture, the cavity of the LNA is significantly larger than other components in the module. Considering the size of the LNA MMIC, it is possible that waveguide modes could propagate in the frequency of operation. This effect could cause instabilities in the amplifier. Several methods exist to reduce this

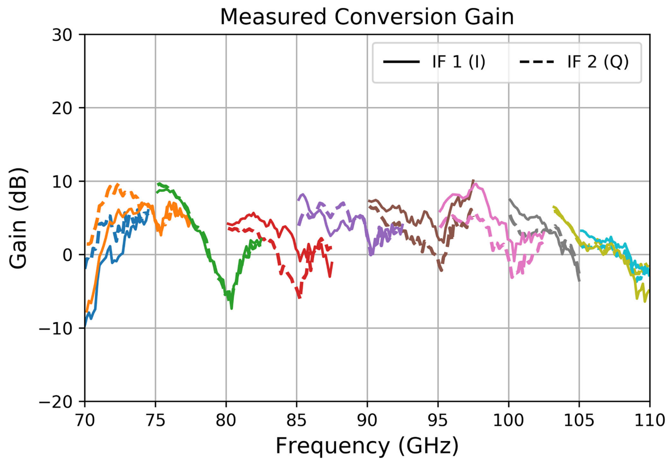

Fig. 12. Measured conversion gain for the I/Q branches for LO frequencies of 33.5, 35, 37.5, 40, 42.5, 45, 47.5, 50, and 52.5 GHz, with an average LO power of 12 dBm.

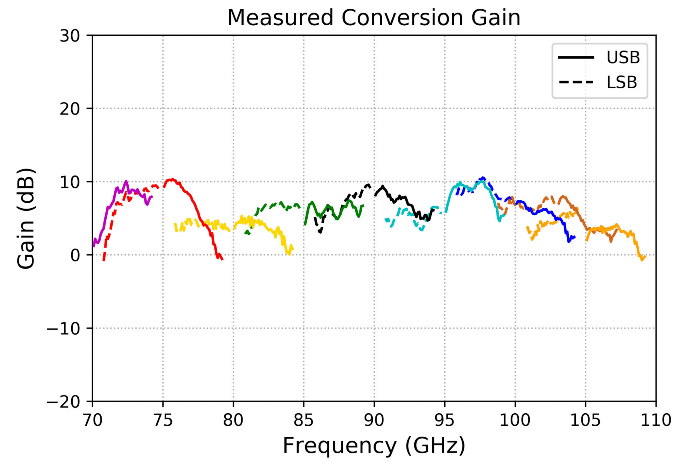

Fig. 13. Measured conversion gain with sideband separation, for LO frequencies of 35, 37.5, 40, 42.5, 45, 47.5, 50, and 52.5 GHz, with an average power of 12.3 dBm.

phenomenon. For this design, the microwave absorber MF-124 from ECCOSORB was placed in the upper side of the cavity.

III. Module Measurements

Several types of measurements were made in order to fully characterize the module.

A. Conversion Gain and Sideband Rejection

Fig. 12 presents the measured conversion gains for the I and Q branches. The decrease in performance around 80 GHz is originated mainly by the performance of the MMIC mixer (see Fig. 6(b) and discussions). Regarding the LO power necessary to drive the entire mixer, if we compare it with the power to drive a single mixer, we would expect an increment of 3 dB (we are now driving two mixers instead of one). However, we detected instead an increase in the LO power of $\sim$5.5 dBm up to 100 GHz and $\sim$7 dBm at higher frequencies. This increment is due to the 1.85 mm connector used to supply the LO and the performance of the microstrip Wilkinson divider, limited by the use of a chip resistor.

The conversion gains of the USB and LSB were measured using an external IF hybrid (see Fig. 13). Although the mixers can work with IF frequencies up to 15 GHz, due to the operating frequency range of the IF hybrid, the measurement was done from 0.8 to 4.2 GHz. An increase in gain is achieved due to the coherent addition of the USB and LSB signals, increasing the performance of the downconverter. This effect can be clearly seen by comparing Figs. 12 and 13, especially between 105 to 110 GHz.

The operating points of the amplifiers were chosen in order to maximize the SRR, effectively canceling small amplitude imbalances in the system. An SRR above 10 dB was achieved in over 75% of the band, as shown in Fig. 14. An illustrative example of this improvement is shown in Fig. 15.

The measurements of the SRR show that there are three regions where it decreases. One is below 75 GHz (not shown here),

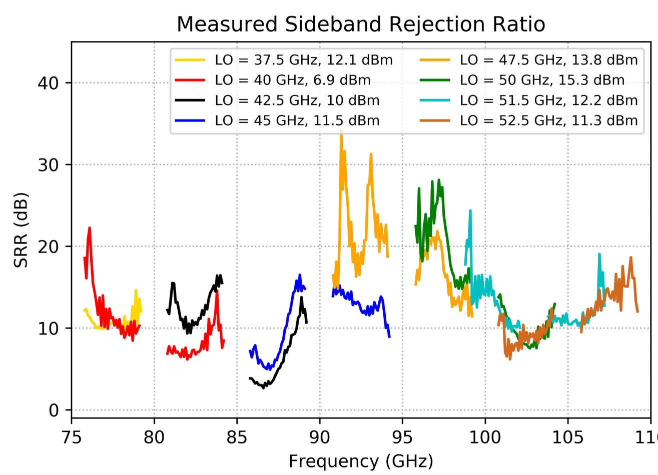

Fig. 14. Measured SRR with an average power of 12.3 dBm.

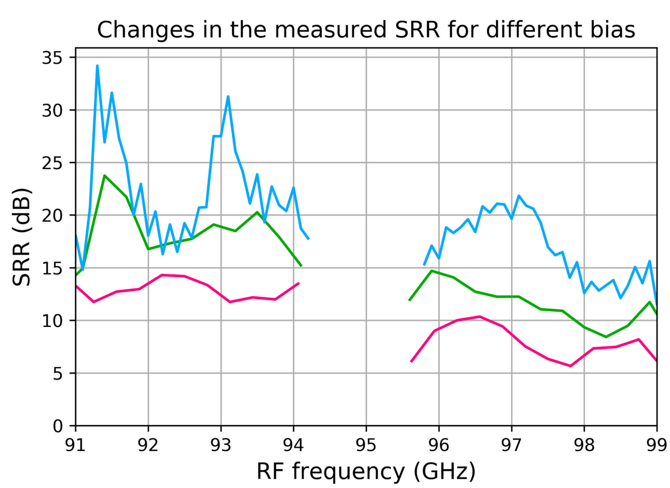

Fig. 15. Examples of SSR improvement with changes in the bias of the amplifiers, for an LO frequency of 47.5 GHz. Magenta: Significantly different bias settings between the amplifiers (50% of power consumption difference). Green: equal bias settings in the amplifiers. Cyan: Optimized bias setting for both amplifiers (10% of power consumption difference).

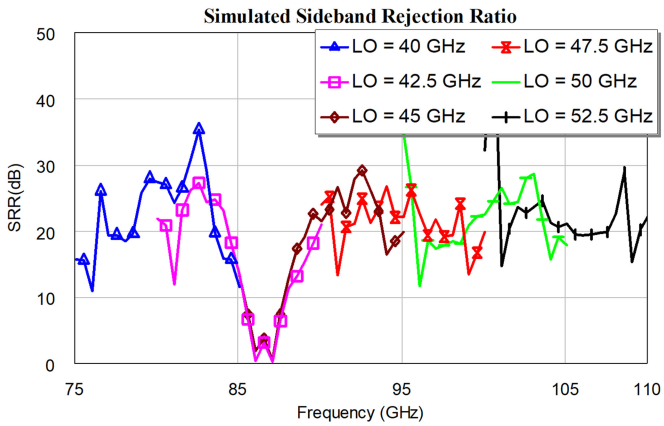

Fig. 16. AWR simulations of the SRR considering the presence of a 96-GHz resonance between the amplifier and the mixer. The degradation around 87 GHz coincides with the experimental results presented in Fig. 14.

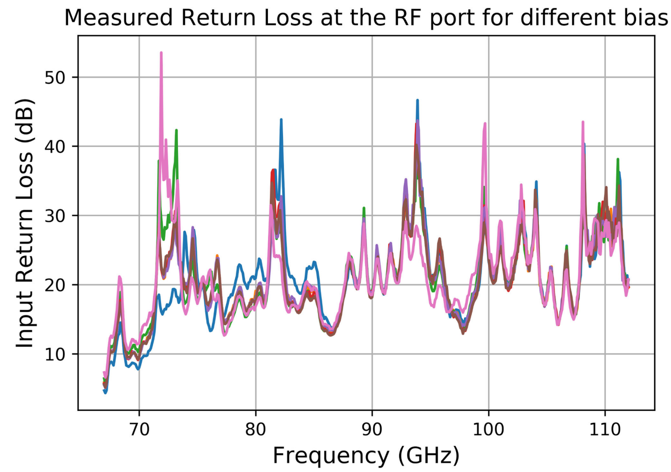

Fig. 17. Measured input return loss of the module for seven different bias settings for an LO of 40 GHz. Some of the bias settings were significantly different to study its effect in the return loss, one example of this is $V_d = 1.2\,\mathrm{V}$ and $I_d = 12\,\mathrm{mA}$ for amplifier A, and $V_d = 2\,\mathrm{V}$ and $I_d = 20\,\mathrm{mA}$ for amplifier B.

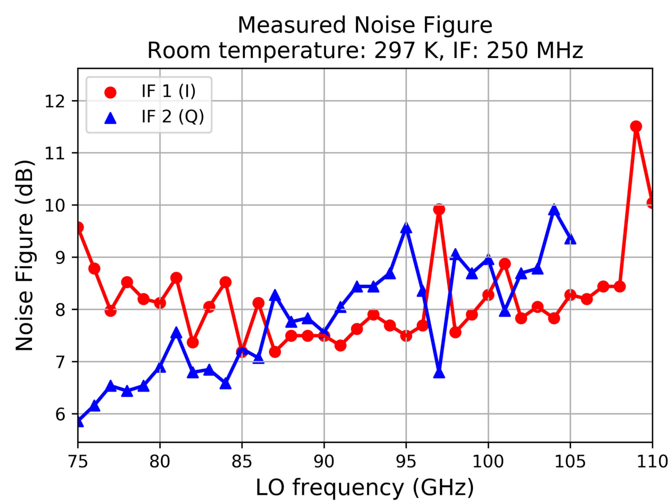

Fig. 18. Measured noise figure of the module for the I and Q branches. These measurements were made using the Y factor method with an integrated spectrum of 250 MHz at room temperature.

due to mechanical constraints in the RF hybrid. The second region of decrease is between 85 and 88 GHz (see Fig. 14). To understand this problem, further analysis was performed using AWR and HFSS. On the one hand, AWR simulations show that an RF resonance between the amplifier and the mixer can cause such behavior. On the other hand, HFSS simulations of the entire cavity where the MMICs are placed show that indeed such resonances appear. Under this circumstance, an interaction between the cavity and the MMICs bondwire can cause this phenomenon. Fig. 16 shows an AWR simulation of the SRR of the entire module considering the presence of the resonance. The figure shows a major downgrade in only a narrow part of the band. It is important to emphasize that this phenomenon is produced by the cavity holding the MMICs and not by the proposed architecture. Possible solutions for this problem are to use a different LNA or implement a gap waveguide structure [19]. The last region of degradation of SRR is between 102 and 104 GHz, this decrease can be explained due to the high input return loss of the amplifier. This phenomenon has been also reported in [15]. Fortunately, there are techniques to increase SSR, such as digital sideband separation [8]. This module was built to be fully compatible with that kind of technique.

B. Return Loss

The input return loss of the module was measured using a spectrum analyzer capable of working up to 112 GHz. The results are presented in Fig. 17, which shows a return loss above 12 dB in the complete band. Similar results were also obtained when using different bias settings for the amplifiers. With the architecture used in this module, the amplifier bias point does not affect the return loss of the module, even using very different bias. Moreover, it should be noted that, because of the very low S_{12} of the LNAs [11], the LO power and frequency do not have an effect in the input return loss of the module. These properties are extremely important in heterodyne receivers based on an LNA as first element. In these types of systems, an isolator is usually placed between the LNA and the down-converting mixer in order to avoid standing waves that originate from the bad output reflection, characteristic of almost all LNAs, and the bad input reflection of most mixers. If possible, isolators are avoided since they are bulky and have limited bandwidth. The results presented here allow this module to be placed after an LNA without the need of an isolator.

C. Noise Figure

Noise measurements for the I and Q branches were made using the Y factor method. A load at room temperature and one submerged into liquid nitrogen were used as hot and cold loads, respectively. The measurements were made at a room temperature of 297 K with an external IF amplifier (30 dB of gain and noise figure of 3 dB) and a detector with an integrated IF spectrum of 250 MHz. The contribution of the IF amplifier to the total noise figure was calculated to be 0.2 dB and, thus, neglected. The results presented in Fig. 18, show a noise figure below 10 dB from 75 to 107 GHz, i.e., in 91% of the desired band. This noise figure at room temperature is sufficient for the module to work as downconverter for applications as atmospheric sciences or mm-wave imaging systems. If low noise is required, it could also be used to provide second-stage amplification.

If extremely low noise is required, as in radio-astronomy applications, the module could be used after a state-of-the-art cryogenic amplifier [20], [21]. Under those circumstances, the low input return losses and the 5 dB gain would allow the use of, e.g., a 30-dB cold-amplification chain with negligible impact on the noise figure of the entire system.

IV. Conclusion

A fully functional 2SB downconverter module, working in the *W* band, has been designed, built, and tested. It has a novel compact architecture that allows obtaining good gain (in average 5 dB) without compromising its return loss (better than 12 dB). This feature allows adding efficiently, if needed, further high-frequency amplification. The module also allows SRR optimization, effectible compensating for any imbalance due to the construction imperfections.

Although the module was designed for operation with a digital IF hybrid, it has been tested with an external analogue hybrid that allowed achieving image rejection of around 10 dB in the majority of the band with some degradation around 87 GHz. Further simulations have demonstrated that this degradation originates from a resonance present in the large cavity needed to place the amplifier and not because of the selected architecture.

Despite the full functionality of the receiver, several upgrades have been identified for future improvements. The most relevant are optimizing the RF hybrid to increase its operational bandwidth [22], a better Wilkinson divider [23] implemented in MMIC format in order to improve the LO range and power performance, and the use of gap waveguides for attenuating resonances in large cavities [19]. Moreover, even its size could be decreased by approximately 30% in the plane perpendicular to the input with a custom waveguide flange or a micro coaxial connector such as the SMPM connector.

The characteristics of the module presented in this article (compactness, excellent return loss, and good gain) make it an excellent choice for integration with multipixel receivers. Areas like astronomy, imaging, telecommunications, or remote sensing can benefit from this development.

References

[1] M. Britcliffe, D. Hoppe, and V. Vilnrotter, "Focal-plane array receiver systems for space communications," *Interplanetary Netw. Progress Rep.*, vol. 42-170, pp. 1–18, 2007.

[2] R. R. G. Güsten *et al.*, "Submillimeter heterodyne arrays for APEX," *Proc. SPIE*, vol. 7020, 2008, Art. no. 702010, doi: 10.1117/12.788271.

[3] K.-F. Schuster *et al.*, "A 230 GHz heterodyne receiver array for the IRAM 30 m telescope," *Astron. Astrophys.*, vol. 423, no 3, pp. 1171–1177, 2004, doi: 10.1051/0004-6361:20034179.

[4] P. J. Sobis, A. Emrich, and J. Stake, "A low VSWR 2SB Schottky receiver," *IEEE Trans. THz Sci. Technol.*, vol. 1, no. 2, pp. 403–411, Nov. 2011, doi: 10.1109/TTHZ.2011.2166176.

[5] A. R. Kerr *et al.*, "In support of instrument technology development for THz astronomy," *Astro2010, Astron. Astrophys. Decadal Surv.*, 2009. [Online]. Available: http://adsabs.harvard.edu/abs/2009astro2010T..29K

[6] K. Devaraj *et al.*, "Argus: A scalable W-band 16-pixel focal plane array for the green bank telescope," in *Proc. Interstellar Medium High Redshift Galaxies Comes Age, NRAO Conf. Ser.*, 2012, vol. 28, pp. 91530P-I–91530P-12, doi: 0.1109/usnc-ursi-nrsm.2014.6928110.

[7] P. Voll *et al.*, "A G-band cryogenic MMIC heterodyne receiver module for astronomical applications," *Int. J. Microw. Wireless Technol.*, vol. 4, no. 3, pp. 283–289, 2012, doi: 10.23919/EuMC.2011.6101883.

[8] R. Finger, P. Mena, N. Reyes, R. Rodriguez, and L. Bronfman, "A calibrated digital sideband separating spectrometer for radio astronomy applications," *Publications Astron. Soc. Pacific*, vol. 125, pp. 263–269, 2013, doi: 10.1086/670175.

[9] J. W. Kooi, "Advanced receivers for submillimeter and far infrared astronomy," Ph.D. thesis, Kapteyn Inst. Astronomy, Rijkuniversiteit Groningen, Groningen, The Netherlands, 2008.

[10] UMS, "Take advantage of very high frequency and cost effective UMS BES Schottky diode process," *Shared Foundry Offer*, 2018. [Online]. Available: https://www.ums-gaas.com/wp-content/uploads/2018/01/2018-Fall-UMS-proposes-a-shared-foundry-run-on-BES-process_Euro2.pdf

[11] OMMIC, "75-110 GHz W-band low noise amplifier," CGY2190UH/C2 Preliminary Datasheet, Feb. 2018. [Online]. Available: http://www.ommic.fr/download/CGY2190UH_C2_PDS_180201.pdf

[12] R. Gawande *et al.*, "W-band IQ sub-harmonic mixers with low LO power for cryogenic operation in large arrays," in *Proc. 9th EuMIC*, Rome, Italy, Oct. 2014, pp. 301–304, doi:10.1109/EuMIC.2014.6997852.

[13] T. H. Lee, *Planar Microwave Engineering*. Cambridge, U.K.: Cambridge Univ. Press, 2004, pp. 338–340, doi:10.1017/cbo9780511812941.

[14] National Instruments Corporation, "Microwave office for MMICs," Microwave Office Application Datasheet, May 2019. [Online]. Available: https://www.awr.com/serve/mmics-datasheet

[15] R. L. Yadava, *Microwave Engineering: Principle and Devices*. Chennai, India: Notion Press, 2018.

[16] D. M. Pozar, *Microwave Engineering*. New York, NY, USA: Wiley, 2012.

[17] Vishay Intertechnology, "High frequency 50 GHz thin film chip resistor," CH Datasheet, Feb. 2019. [Online]. Available: https://www.vishay.com/docs/53014/ch.pdf

[18] A. Khudchenko, R. Hesper, A. M. Baryshev, J. Barkhof, and F. P. Mena, "Modular 2SB SIS receiver for 600-720 GHz: Performance and characterization methods," *IEEE Trans. THz Sci. Technol.*, vol. 7, no. 6, pp. 686–693, Nov. 2017, doi: 10.1109/TTHZ.2017.2758270.

[19] A. U. Zaman, M. Alexanderson, T. Vukusic, and P. S. Kildal, "Gap waveguide PMC packaging for improved isolation of circuit components in high-frequency microwave modules," *IEEE Trans. Compon., Packag. Manuf. Technol.*, vol. 4, no. 1, pp. 16–25, Jan. 2014, doi: 10.1109/TCPMT.2013.2271651.

[20] Y. Tang *et al.*, "Cryogenic W-band LNA for ALMA band 2 + 3 with average noise temperature of 24 K," in *Proc. IEEE MTT-S Int. Microw. Symp.*, 2017, pp. 176–179, doi: 10.1109/mwsym.2017.8058981.

[21] D. Cuadrado-Calle *et al.*, "Broadband MMIC LNAs for ALMA band 2 + 3 with noise temperature below 28 K," *IEEE Trans. Microw. Theory Techn.*, vol. 65, no. 5, pp. 1589–1597, May 2017, doi: 10.1109/tmtt.2016.2639018.

[22] J. Ding, Y. Zhao, J. X. Ge, and S. Shi, "A 90° waveguide hybrid with low amplitude imbalance in full W-band," *J. Infrared, Millimeter, THz Waves*, vol. 40, no. 4, pp. 429–434, Apr. 2019, doi: 10.1007/s10762-019-00577-1.

[23] F. Xu, G. Guo, E. Li, and J. Wu, "An ultra-broadband 3-dB power divider," in *Proc. 5th Global Symp. Millimeter-Waves*, May 2012, pp. 347–350, doi: 10.1109/GSMM.2012.6314071.

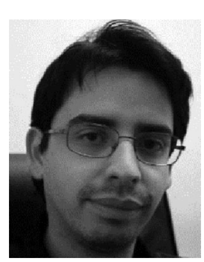

David Monasterio received the B.S. degree in electrical engineering and the professional degree of electrical civil engineer in microwave engineering from the Universidad de Chile, Santiago, Chile, in 2010 and 2013, respectively.

Since 2013, he has been with the Millimeter Wave Laboratory, Universidad de Chile. His research interests include radio astronomy instrumentation, planar antennas, phased array, local oscillators, antenna beam pattern measurements, passive microwave components, microwave mixers, and monolithic microwave integrated circuit.

Claudio Jarufe received the graduation degree in electrical engineering, the M.S. degree in physics, and the Ph.D. degree in electric engineering from the Universidad de Chile, Santiago, Chile, in 2011, 2012, and 2018 respectively.

In 2013, he did an internship with the Yebes Observatory, Spain, developing low noise amplifiers at Q-band. During his Ph. D. degree, he developed millimeter wave electronics for heterodyne receivers at GHz frequencies. His research interests include cryogenic low noise amplifiers and receivers, microwave integrated circuits, microwave mixers, wideband antennas, and compact heterodyne cameras.

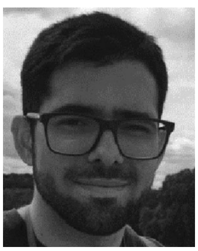

Diego Gallardo was born in Santiago, Chile, in 1996. He is currently studying B.S. degree in electrical engineering and the professional degree of electrical civil engineer at the Physical and Mathematical Sciences Faculty, Universidad de Chile, Santiago, Chile.

His research interests include the design and construction of electromagnetic devices in the microwave band, with a strong interest in antennas.

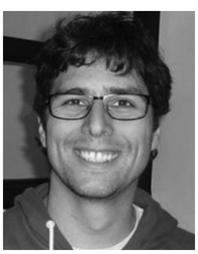

Nicolas Reyes received the Ph.D. degree in electrical engineering from the Universidad de Chile, Santiago, Chile, in 2012.

From 2008 to 2012, he was involved in the design of the ALMA Band 1 instrument (35–50 GHz). In 2013, he joined the Max Planck Institute for Radio Astronomy, Bonn, Germany, as a Postdoctoral Researcher for the SOFIA observatory. He worked in terahertz instrumentation for astronomy, specifically in the development of UpGREAT, the first supra-THz heterodyne camera at 1.9 THz. In 2015, he joined as an Assistant Professor the Department of Electrical Engineering, Universidad de Chile. Since 2019, he has been an Instrument Scientist with the Max Planck Institute for Radio Astronomy, Bonn, Germany, in the sub-mm technology division. He works on the design of astronomical instrumentation for ALMA and other projects as CCAT-p. His research interests include microwave circuits, low-noise electronic, antennas, numerical simulation, optics, and radio astronomy instrumentation.

Fausto Patricio Mena received the B.S. degree in physics from Escuela Politécnica Nacional, Quito, Ecuador, in 1994, and the M.S. and Ph.D. degrees in physics from the University of Groningen, Groningen, The Netherlands, in 2000 and 2004, respectively.

In 2004, he joined as an Instrument Scientist at the Low Energy Division, Netherlands Institute for Space Research, Groningen, The Netherlands. In 2008, he moved to the Universidad de Chile, Santiago, Chile, where he co-founded the Radio Astronomical Instrumentation Group and the Millimeter Wave Laboratory. He is currently an Associate Professor with the Department of Electrical Engineering, Universidad de Chile. His research interests include the design, construction, and testing of components and systems for millimeter and submillimeter wave instrumentation.

Leonardo Bronfman was born in Santiago, Chile, in 1954. He received the M.Sc. degree in physics from the Universidad de Chile, Santiago, Chile, in 1980, and the Ph.D. degree in astrophysics from Columbia University, New York, NY, USA, in 1986, with the first complete CO Survey of the Southern Milky Way.

Since 1998, he has been a Full Professor with the Department of Astronomy, Universidad de Chile. He was the Department Chairman in 1993–1996, and in 2005–2008. Earlier in his career, he was an Associate Researcher with ESO (1990–1991), Visiting Scientist with NAOJ (1996), and Visiting Scientist with NRAO (1998). His research interests inlude Galactic ISM, massive star formation, and mm-wave instrumentation.

Dr. Bronfman has been, since 2008, PI for Astronomical Instrumentation with the Center of Excellence for Astrophysics and Related Technologies, Universidad de Chile, where he led the implementation of the Mm-wave Laboratory at the Cerro Calán National Astronomical Observatory. The Millimeter Wave Laboratory, Universidad de Chile developed a prototype receiver for ALMA Band 1, and is presently producing the optics for the full ALMA Band 1 receiver suit.